

# The average local ionization energy as a tool for identifying reactive sites on defect-containing model graphene systems

Jane S. Murray · Zenaida Peralta-Inga Shields · Pat Lane · Laura Macaveiu · Felipe A. Bulat

Received: 30 August 2012 / Accepted: 12 November 2012 / Published online: 30 November 2012  
© Springer-Verlag Berlin Heidelberg 2012

**Abstract** In a continuing effort to further explore the use of the average local ionization energy  $\bar{I}(\mathbf{r})$  as a computational tool, we have investigated how well  $\bar{I}(\mathbf{r})$  computed on molecular surfaces serves as a predictive tool for identifying the sites of the more reactive electrons in several nonplanar defect-containing model graphene systems, each containing one or more pentagons. They include corannulene ( $C_{20}H_{10}$ ), two inverse Stone-Thrower-Wales defect-containing structures  $C_{26}H_{12}$  and  $C_{42}H_{16}$ , and a nanotube cap model  $C_{22}H_6$ , whose end is formed by three fused pentagons. Coronene ( $C_{24}H_{12}$ ) has been included as a reference planar defect-free graphene model. We have optimized the structures of these systems as well as several monohydrogenated derivatives at the B3PW91/6-31G\* level, and have computed their  $\bar{I}(\mathbf{r})$  on molecular surfaces corresponding to the 0.001 au, 0.003 au and 0.005 au contours of the electronic density. We find that (1) the convex sides of the interior carbons of the nonplanar models are more reactive than the concave sides, and (2) the magnitudes of the lowest  $\bar{I}(\mathbf{r})$  surface minima (the  $\bar{I}_{S,\min}$ ) correlate well with the interaction energies for hydrogenation at these sites. These  $\bar{I}_{S,\min}$  values decrease in magnitude as the nonplanarity of the site increases, consistent with earlier studies. A practical benefit of the use of  $\bar{I}(\mathbf{r})$  is that a single calculation suffices to characterize the numerous sites on a large molecular system, such as graphene and defect-containing graphene models.

**Keywords** Average local ionization energy · Defect-containing graphene model · Corannulene · Inverse Stone-Thrower-Wales defect · Molecular surface · Reactive site · Hydrogenation

## Introduction

The average local ionization energy  $\bar{I}(\mathbf{r})$  was introduced in 1990 by Sjöberg et al. [1] as a means of identifying and ranking the sites of the more reactive electrons in a molecular system.  $\bar{I}(\mathbf{r})$  is given by Eq. (1):

$$\bar{I}(\mathbf{r}) = \frac{\sum_i \rho_i(\mathbf{r}) |\varepsilon_i|}{\rho(\mathbf{r})} \quad (1)$$

In Eq. (1),  $\rho_i(\mathbf{r})$  is the electronic density of orbital  $i$ , having energy  $\varepsilon_i$ , at the point  $\mathbf{r}$  of interest;  $\rho(\mathbf{r})$  is the total electronic density of the system. The summation is over all occupied orbitals.

Within the framework of Hartree-Fock formalism, and with the support of Koopmans' theorem [2, 3],  $\bar{I}(\mathbf{r})$  can be interpreted as the energy required to remove an electron from the system at the point  $\mathbf{r}$ . The focus is on the point in space  $\mathbf{r}$ , relevant to chemical reactivity, which is local, i.e., site-specific, rather than upon a particular orbital. Equation (1) can also be applied within the context of density functional theory [4]; the magnitudes of the Kohn-Sham  $\bar{I}(\mathbf{r})$  differ from the Hartree-Fock but the trends are generally similar.

The highlight of the first application of  $\bar{I}(\mathbf{r})$  was that, when computed on an appropriate molecular surface,  $\bar{I}(\mathbf{r})$  accounted for both the qualitative identification of the reactive carbons on a particular substituted aromatic and the quantitative ranking of these sites among the series of

J. S. Murray (✉) · Z. P.-I. Shields · P. Lane · L. Macaveiu  
CleveTheoComp, 1951 W. 26th Street, Suite 409,  
Cleveland, OH 44113, USA  
e-mail: jsmurray@uno.edu

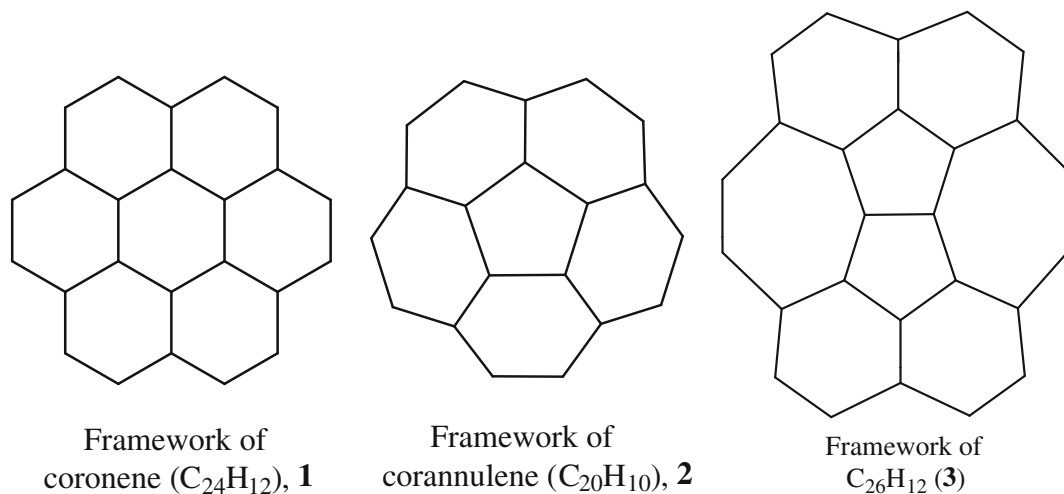
F. A. Bulat  
Fable Theory and Computation, Washington, DC 20009, USA

$C_6H_5X$  molecules, as evidenced by an excellent correlation with the Hammett constants [1]. The further use of  $\bar{I}(\mathbf{r})$  in studies involving chemical reactivity was subsequently explored in a series of papers [5–9]; these included studies examining the ability of  $\bar{I}(\mathbf{r})$  to correlate with protonation enthalpies and  $pK_a$  values, in azines and azoles [6] and in first-row acids [7, 8]. Its ability to show the shell structure of atoms was identified already in 1991 [10], and its effectiveness as a means of obtaining a relative scale of atomic electronegativities has been demonstrated more recently [11, 12]. In the 22 years since the introduction of  $\bar{I}(\mathbf{r})$  as a computational tool, its applications have grown, as reviewed by Politzer et al. [13, 14].

One of the important realizations regarding the use of  $\bar{I}(\mathbf{r})$  as a computational tool in studies of sites for electrophilic attack was noted in 1993 by Brinck et al. [13] in a study exploring the  $pK_a$ s and protonation enthalpies of the first through third row Group V–VII hydrides. It was found that  $\bar{I}(\mathbf{r})$  is used most successfully in a complementary manner with the electrostatic potential  $V(\mathbf{r})$  [15, 16], with  $V(\mathbf{r})$  dominating the approach of reactants to one another and  $\bar{I}(\mathbf{r})$  governing the location for the possible reaction between electrophile and electrophilic site. The use of both  $V(\mathbf{r})$  and

$\bar{I}(\mathbf{r})$  is particularly important when comparing atoms from different rows of the periodic table [15, 17]. However, in studies comparing similar atoms, such as carbons in polycyclic aromatic hydrocarbons [18], model graphene systems [19, 20], and model carbon nanotubes [21, 22], the exclusive use of  $\bar{I}(\mathbf{r})$  has been shown to be effective in determining reactive sites.

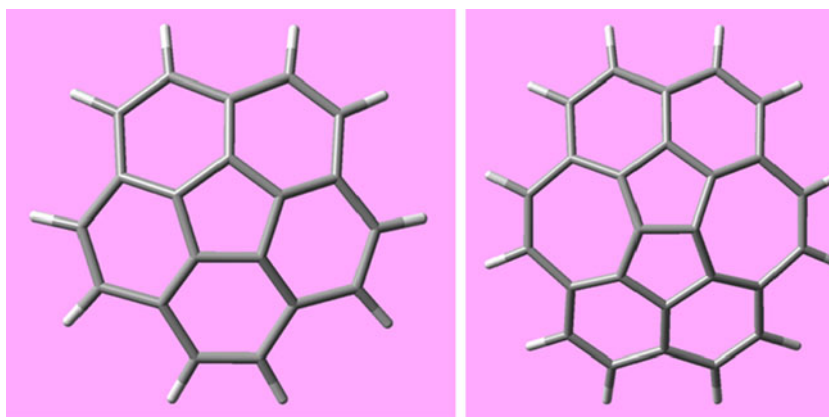
A useful feature in the utilization of  $\bar{I}(\mathbf{r})$  for identifying regions within molecular systems with reactive electrons, particularly in studies of large frameworks, is that one calculation suffices to characterize multiple sites in the same system [18–22]. This is in comparison to performing tens to hundreds of calculations to obtain, for example, interaction energies at the various sites on a large framework. Recent applications exploiting this time-efficient and practical feature of  $\bar{I}(\mathbf{r})$  include its use in finding the favored sites for: (1) first hydrogenation and fluorination on a Stone-Wales defect-containing (5,5) model carbon nanotube [21]; (2) the first and second hydrogenation and fluorination in graphene model systems (such as coronene,  $C_{24}H_{12}$ , **1**) [20]; and (3) second chlorination on a (5,5) carbon nanotube model system [22].



In the present study, we are extending our analysis of  $\bar{I}(\mathbf{r})$  of large carbon frameworks to defect-containing model graphene systems **2** (corannulene,  $C_{20}H_{10}$ ) and **3** ( $C_{26}H_{12}$ ), shown above and in Fig. 1, and **4** ( $C_{42}H_{16}$ ) and **5** ( $C_{22}H_6$ ), given in Fig. 2. Systems **2–5** differ from pristine graphene models such as **1** in that each has one or more pentagons in its framework and subsequently is nonplanar. Corannulene, **2**, is simply a pentagon with five hexagonal rings fused to it [23–25]; since it can be viewed as being part of fullerene ( $C_{60}$ ),

it is often called a “bucky bowl” [26]. Compounds **3** and **4** are models containing the inverse Stone-Thrower-Wales defect [27–29]: two fused pentagons that are then fused to two heptagons [30]; **5** can be viewed as a nanotube cap with three fused pentagons at its end and alternating pentagonal and hexagonal rings along its sides [31]. The presence of pentagons and heptagons can be viewed as structural defects. We included coronene (**1**) in our analysis to serve as a reference point for graphenic-like carbons [20, 32–35].

**Fig. 1** Molecular frameworks of corannulene (**2**) (left) and inverse Stone-Thrower-Wales defective graphene model **3** (right)



We attached a hydrogen computationally to some of the interior carbon sites of **1–5**, including both sites on the convex (outer) and concave (inner) sides of **2** and **3**. Our overall objectives were to assess the effectiveness of  $\bar{I}(\mathbf{r})$  in (1) finding the most reactive carbon(s) within a particular carbon system (i.e., **3**) and (2) ranking the most reactive sites within a series of systems (i.e., **1–5**). We also looked at possible second hydrogenation sites on these systems.

## Methods

We carried out geometry optimizations of **1–5** and some monohydrogenated derivatives of **1–5** at the B3PW91/6-31G\* level using Gaussian 09 [36]. Gaussian 09 wavefunction files have served as input for the Wave Function Analysis–Surface Analysis Suite (WFA-SAS) [37], used for computing  $\bar{I}(\mathbf{r})$  for **1–5** and their most stable monohydrogenated derivatives.

In using  $\bar{I}(\mathbf{r})$  to analyze reactive behavior, it is typically computed on the surface of the molecule and labeled  $\bar{I}_S(\mathbf{r})$ . The surface has often been taken to be the 0.001 au (electrons/bohr<sup>3</sup>) contour of the molecule's electronic density, as proposed by Bader et al. [38]. The points at which  $\bar{I}(\mathbf{r})$  has its lowest values are of particular interest; these are designated as  $\bar{I}_{S,\min}$  and are indicative of the locations of the least-tightly-bound, most reactive electrons [1, 14]. In this study, we have

computed  $\bar{I}_S(\mathbf{r})$  on molecular surfaces corresponding to the 0.001 au contour of the electronic density. We have in addition provided some comparisons to  $\bar{I}_S(\mathbf{r})$  computed on 0.003 au and 0.005 au surfaces.

We attached hydrogens at selected interior carbons of **1–5** that have  $\bar{I}_{S,\min}$ ; these hydrogenated structures are designated **1H**, **2H**, **3H**, **4H** and **5H**. The interaction energies for their formation are given by

$$\Delta E (\mathbf{1H}, \mathbf{2H}, \mathbf{3H}, \mathbf{4H} \text{ or } \mathbf{5H}) = E (\mathbf{1H}, \mathbf{2H}, \mathbf{3H}, \mathbf{4H} \text{ or } \mathbf{5H}) - E(\mathbf{1}, \mathbf{2}, \mathbf{3}, \mathbf{4} \text{ or } \mathbf{5}) - E(\text{H}) \quad (2)$$

in which the terms correspond to energy minima at 0 K.

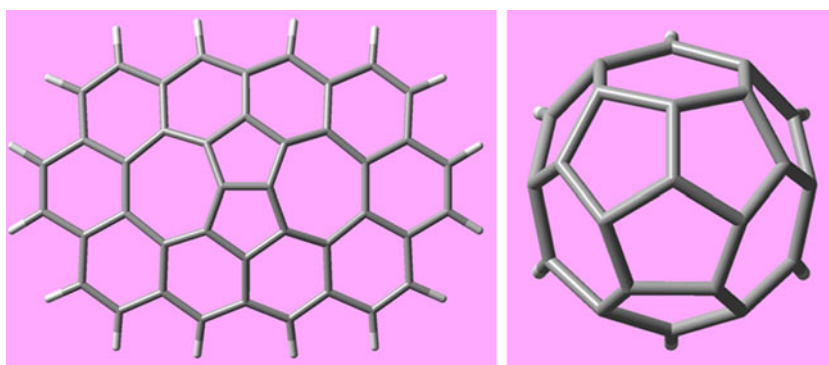
## Results

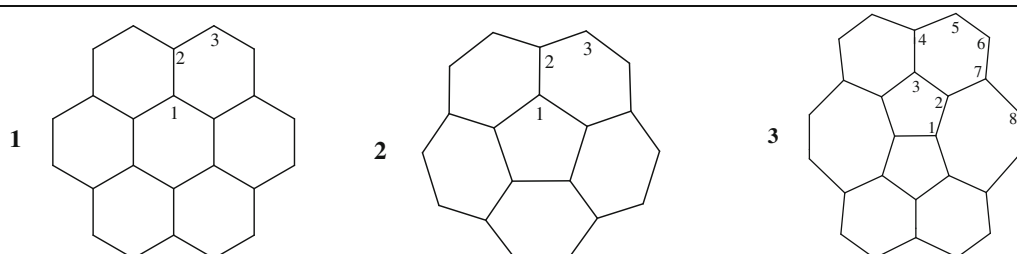
### Nonfunctionalized systems **1–3**

The optimized B3PW91/6-31G\* C–C bond lengths of **1–3** are given in Table 1 along with the positions and values of the  $\bar{I}_{S,\min}$  found on the 0.001 au molecular surfaces of **1–3**. We will look first at the structures and then at the  $\bar{I}_S(\mathbf{r})$  data.

In planar coronene (**1**), for which the interior carbons have been taken in earlier studies as models for pristine graphenic carbons [20, 32–35], the C<sub>1</sub>–C<sub>1</sub>, C<sub>1</sub>–C<sub>2</sub> and C<sub>2</sub>–C<sub>3</sub> bonds range from 1.419 Å to 1.425 Å, bracketing the experimental 1.420 Å of graphene [39]. The peripheral C<sub>3</sub>–

**Fig. 2** Molecular frameworks for inverse Stone-Thrower-Wales defective graphene model **4** (left) and nanotube cap model **5** containing three central fused pentagons (right)



**Table 1** Computed bond lengths and  $\bar{I}_{S,\min}$  values (at the 0.001 au contour of the electronic density) for the carbons of nonfunctionalized systems 1–3.  $\bar{I}_{S,\min}$  values for both the convex and concave sides of 2 and 3 are listed


Molecule	Bond	Length (Å)	Planar sides		Convex side		Concave side	
			Position	$\bar{I}_{S,\min}$ (eV)	Position	$\bar{I}_{S,\min}$ (eV)	Position	$\bar{I}_{S,\min}$ (eV)
<b>1</b>	C <sub>1</sub> -C <sub>1</sub>	1.425	C <sub>1</sub>	9.89				
	C <sub>1</sub> -C <sub>2</sub>	1.419	C <sub>2</sub>	9.89				
	C <sub>2</sub> -C <sub>3</sub>	1.422	C <sub>3</sub> -C <sub>3</sub>	8.98				
	C <sub>3</sub> -C <sub>3</sub>	1.371						
<b>2</b>	C <sub>1</sub> -C <sub>1</sub>	1.414			C <sub>1</sub>	9.24	C <sub>1</sub>	none
	C <sub>1</sub> -C <sub>2</sub>	1.383			C <sub>3</sub> -C <sub>3</sub>	8.85	C <sub>3</sub> -C <sub>3</sub>	8.95
	C <sub>2</sub> -C <sub>3</sub>	1.445						
	C <sub>3</sub> -C <sub>3</sub>	1.388						
<b>3</b>	C <sub>1</sub> -C <sub>1</sub>	1.389			C <sub>1</sub>	8.08	C <sub>1</sub>	none
	C <sub>1</sub> -C <sub>2</sub>	1.428			C <sub>4</sub>	9.13	C <sub>2</sub>	10.21
	C <sub>2</sub> -C <sub>3</sub>	1.419			C <sub>7</sub>	9.63	C <sub>3</sub>	10.09
	C <sub>3</sub> -C <sub>4</sub>	1.394			C <sub>5</sub> -C <sub>6</sub>	8.95	C <sub>5</sub> -C <sub>6</sub>	9.05
	C <sub>4</sub> -C <sub>5</sub>	1.430			C <sub>8</sub> -C <sub>8</sub>	8.80	C <sub>8</sub> -C <sub>8</sub>	8.98
	C <sub>5</sub> -C <sub>6</sub>	1.389						
	C <sub>6</sub> -C <sub>7</sub>	1.437						
	C <sub>7</sub> -C <sub>8</sub>	1.460						
C <sub>8</sub> -C <sub>8</sub>	1.375							

C<sub>3</sub> bonds are, however, 1.371 Å, indicating considerable double bond character [40]. The presence of a pentagonal ring in corannulene (**2**) and two fused pentagonal rings and the adjoining heptagonal rings in inverse Stone-Thrower-Wales defect-containing model **3** introduces more variation in the computed C–C bond lengths, with the five central C<sub>1</sub>–C<sub>1</sub> bonds in **2** and the C<sub>1</sub>–C<sub>1</sub> bond in **3** shortened relative to those of **1** (1.425 Å) to 1.414 Å and 1.389 Å, respectively. The peripheral C<sub>3</sub>–C<sub>3</sub> bonds in **2** and the C<sub>5</sub>–C<sub>6</sub> and C<sub>8</sub>–C<sub>8</sub> bonds in **3** are similar to those of **1**, again indicative of significant double bond character.

Looking next at the  $\bar{I}_{S,\min}$  of **1–3** in Table 1 and plots of  $\bar{I}_S(\mathbf{r})$  for **2** and **3** shown in Figs. 3 and 4 brings out the fact that the nonplanar **2** and **3** have nonequivalent convex (outer) and concave (inner) sides, which exhibit differing site reactivities, unlike the planar **1** for which the  $\bar{I}_S(\mathbf{r})$  of both sides is the same [20]. Figures 3 and 4 and Table 1 show the general feature that the convex sides of **2** and **3** have more reactive electrons (lower  $\bar{I}_{S,\min}$ ) in the interior regions than do the concave sides. Perhaps the most striking difference between the two sides of **2** and **3** is that the C<sub>1</sub> carbons show no  $\bar{I}_{S,\min}$  on the concave side. Compound **3** does have  $\bar{I}_{S,\min}$  at positions C<sub>2</sub> and C<sub>3</sub> of its concave side; the magnitudes of these  $\bar{I}_{S,\min}$  are, however, higher than the

graphenic-like C<sub>1</sub> carbons of **1**. The C<sub>1</sub>  $\bar{I}_{S,\min}$  on the planar or convex sides of **1–3** decrease from ~9.9 eV in **1** to ~9.2 eV in **2** to ~8.1 eV in **3**, indicating an increase in the reactivities of the electrons at these sites in going from **1** to **3**.

Systems **1–3** each have  $\bar{I}_{S,\min}$  associated with their peripheral shorter C–C bonds, consistent with earlier studies showing  $\bar{I}_{S,\min}$  for C–C bonds having partial or full double bond character [14, 18–22]. Since our interest is in the more graphenic-like carbons of model systems **1–3**, we will focus on the interior sites in the remainder of this study.

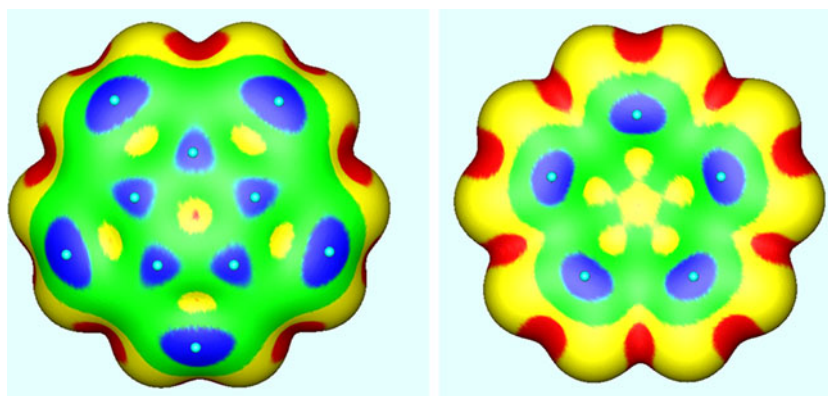
#### Identification of sites for first hydrogenation

##### Interior carbon sites of **1–3**

In earlier studies of large carbon framework systems, including graphene models coronene **1** and C<sub>54</sub>H<sub>18</sub> [20], a Stone-Wales defective (5,5) nanotube model [21] and a chlorinated pristine (5,5) nanotube model [22], we have shown that the most favorable sites for hydrogenation, fluorination or further chlorination, as measured by the reaction energies, tend to be those bearing  $\bar{I}_{S,\min}$ . In view of this finding, Table 2 lists the  $\bar{I}_{S,\min}$  for the interior carbons of **1–3** and the reaction energies at 0 K for hydrogenation at these sites.



**Fig. 3** Computed  $\bar{I}_S(\mathbf{r})$  on the 0.001 au molecular surface of coronene (**2**). *Left view* Convex surface, *right view* concave surface. Color ranges (eV): blue < 9.5; green 9.5–11.0; yellow 11.0–12.0; red > 12.0. The locations of the  $\bar{I}_{S,\min}$  with values less than 9.5 eV are indicated by light blue hemispheres



Our computed B3PW91/6-31G\*  $\Delta E$  for hydrogenation at  $C_1$  of coronene (**1**),  $-14.5 \text{ kcal mol}^{-1}$ , compares well with values obtained in earlier studies carried out at higher computational levels (which range from  $-13.6 \text{ kcal mol}^{-1}$  to  $-15.1 \text{ kcal mol}^{-1}$ ) [20, 33, 35]. We find that as  $\bar{I}_{S,\min}$  of  $C_1$  decreases in going from **1** to **2** to **3**, the  $\Delta E$  for hydrogenation at those sites become more negative;  $\Delta E$  for hydrogenation at  $C_1$  on the convex sides of **2** and **3** are  $-48.0$  and  $-60.1 \text{ kcal mol}^{-1}$ , respectively.

A point of interest is that if a hydrogen is attached to  $C_1$  on the concave side of **2** or **3**, a position that does not have an  $\bar{I}_{S,\min}$  in either model, then the optimization of each proceeds with an inversion of the structure to yield a product with the hydrogen on the convex side of the system; see **2H** and **3H** in Fig. 5. However, hydrogenation at the sites of the  $\bar{I}_{S,\min}$  on the concave side of **3** ( $C_2$  and  $C_3$ ) yields structures with hydrogens attached to the concave surface, with  $\Delta E$  of  $-14.2$  and  $-8.0 \text{ kcal mol}^{-1}$ , respectively. The latter are similar or less than for hydrogenation of  $C_1$  in coronene. Overall, the trends in the  $\Delta E$  follow those of the  $\bar{I}_{S,\min}$ .

#### $C_1$ sites of **1–5**

The data in Table 3 explore further the relationship between our computed  $\bar{I}_{S,\min}$  at  $C_1$  of **1–5** and the energies of hydrogenation at the sites of these  $\bar{I}_{S,\min}$ . Figure 6 shows

that the most reactive carbons in the larger inverse Stone-Thrower-Wales defect-containing model **4** are predicted to be the  $C_1$  carbons, as was found for the smaller model **3**; these predictions are consistent with those of by Lusk et al. [29] for inverse Stone-Thrower-Wales defect-containing graphene models. In **5**, the central carbon  $C_1$  is found to be the most reactive (Table 3), in agreement with an earlier study pointing out that the regions of most negative electrostatic potential and lowest  $\bar{I}_S(\mathbf{r})$  of a (6,0) nanotube model with a cap structure containing model **5** are associated with  $C_1$  [31]. As noted in the last section, we see that, as  $\bar{I}_{S,\min}$  decreases in magnitude, the  $\Delta E$  become more negative. In fact, there is a good linear correlation between  $\bar{I}_{S,\min}$  and  $\Delta E$  for the systems **1–5**, with linear correlation coefficient  $R=0.958$ .

In Table 3, we use the sums of the  $C-C_1-C$  angles in **1–5** as measures of the systems' planarities. The sum would be  $360^\circ$  for perfect planarity, as we find in coronene (**1**) before hydrogenation. Table 3 shows that the  $C_1$   $\bar{I}_{S,\min}$  decrease in the same order as do the sums of the  $C-C_1-C$  angles, indicating that these sites become more reactive as the local planarity decreases, consistent with earlier studies [21, 30, 31, 41, 42].

Since  $\bar{I}_S(\mathbf{r})$  data pertain to the systems **1–5** prior to reaction, our  $\bar{I}_{S,\min}$  cannot reflect factors that may result

**Fig. 4** Computed  $\bar{I}_S(\mathbf{r})$  on the 0.001 au molecular surface of inverse Stone-Thrower-Wales defect-containing model **3**. *Left view* Convex surface, *right view* concave surface. Color ranges (eV): blue < 9.5; green 9.5–11.0; yellow 11.0–12.0; red > 12.0. The locations of the  $\bar{I}_{S,\min}$  with magnitudes less than 10.5 eV are given by light blue hemispheres

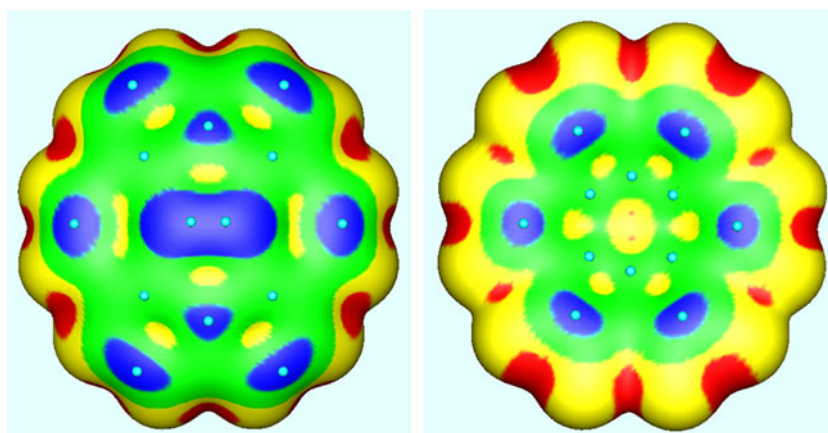


**Table 2** Computed 0.001 au  $\bar{I}_{S,\min}$  values for interior carbons of **1–3** and reaction energies  $\Delta E$  at 0 K for hydrogenation at the sites of these  $\bar{I}_{S,\min}$  to form **1H**, **2H** and **3H**. Numbering of sites in **1–3** as in Table 1

Molecular system	Site	$\bar{I}_{S,\min}$ (eV)	$\Delta E$ (kcal mol <sup>-1</sup> )
<b>1</b>	C <sub>1</sub>	9.89	-14.46
<b>2</b>	Convex C <sub>1</sub>	9.24	-47.95
<b>3</b>	Convex C <sub>1</sub>	8.08	-60.06
	Concave C <sub>2</sub>	10.21	-14.19
	Concave C <sub>3</sub>	10.09	-8.03

from the reaction, such as additional strain/stabilization, interatomic repulsion, etc. This has been pointed out earlier [20, 22]. It is, therefore, perhaps useful to look in Table 3 at the sums of the C–C<sub>1</sub>–C angles after hydrogenation at C<sub>1</sub>. For each system, this sum is less than before hydrogenation (also given in Table 3), with the differences in these sums before and after hydrogenation ranging from 17° to 29°. While this is a fairly narrow range, it is noteworthy that the correlation between  $\Delta E$  and  $\bar{I}_{S,\min}$  can be improved by writing  $\Delta E$  as a function of both  $\bar{I}_{S,\min}$  and the sum of the C–C<sub>1</sub>–C angles *after* hydrogenation at C<sub>1</sub>.

As a point of practical interest, we present in Table 4 a comparison of the  $\bar{I}_{S,\min}$  values at C<sub>1</sub> of **1–5** on molecular surfaces corresponding to the 0.001 au, 0.003 au and 0.005 au contours of the electronic density. The  $\bar{I}_{S,\min}$  values increase for each system as one progresses from the 0.001 au to the higher contours of the electronic density; this reflects greater contributions from orbitals closer to the nucleus with orbital energies of greater magnitudes. At the 0.001 au contour of the electronic density, the distances from carbon C<sub>1</sub> to the surface minima are ~2.0 Å, greater than the van der Waals radius of carbon (1.70 Å), while at the 0.003 au and 0.005 au contours, the distances are ~1.69 Å and ~1.55 Å, respectively. The trends shown by the  $\bar{I}_{S,\min}$  values of **1** to **5** at the three contours are similar; this suggests that contours in the 0.001 au to 0.005 au range will provide realistic surfaces for identification of sites with the most reactive electrons. In some situations, larger contours of the electronic density that yield surfaces closer to the nuclei of the molecule may allow better visualization of sites for second reactions [22].

**Fig. 5** Molecular frameworks for hydrogenated corannulene **2H** (left) and hydrogenated inverse Stone-Thrower-Wales defective graphene model **3H** (right). The hydrogen in each is attached to one of the C<sub>1</sub> carbons

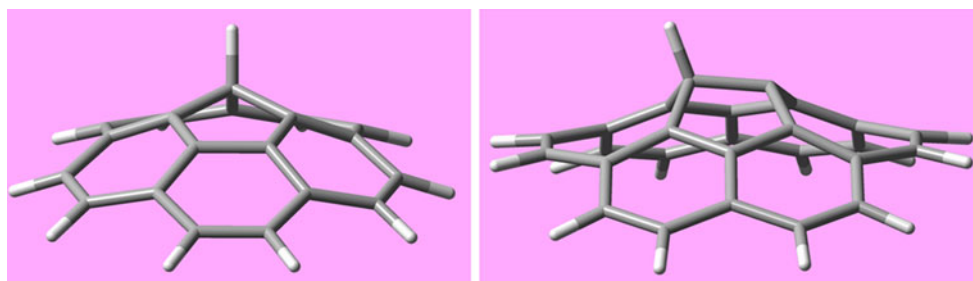


**Table 3** Computed 0.001 au  $\bar{I}_{S,\min}$  values at positions corresponding to C<sub>1</sub> of **1–5**, reaction energies at 0 K for hydrogenation at the sites of these  $\bar{I}_{S,\min}$ , summation of C–C<sub>1</sub>–C angles before hydrogenation and summation of C–C<sub>1</sub>–C angles after hydrogenation. Position of C<sub>1</sub> corresponds to the numbering given in Table 1 for **1–3**. For **4**, C<sub>1</sub> corresponds to the carbons that are members of the two fused pentagons, as in **3**. In **5**, C<sub>1</sub> is the central carbon

Molecule	$\bar{I}_{S,\min}$ (eV)	$\Delta E$ (kcal mol <sup>-1</sup> )	$\sum$ C–C <sub>1</sub> –C without H	$\sum$ C–C <sub>1</sub> –C with H
<b>1</b>	9.89	-14.46	360.0	343.3
<b>2</b>	9.24	-47.95	354.0	326.5
<b>3</b>	8.08	-60.06	346.0	317.3
<b>4</b>	8.14	-61.74	347.6	319.5
<b>5</b>	7.49	-83.70	317.5	300.9

Finally, we mention that the  $\bar{I}_{S,\min}$  values at C<sub>1</sub> of **1–5** have contributions from the highest-occupied molecular orbital (HOMO) ranging from near zero in **1**, **4** and **5** to an average of 20 % in **2** for the highest two degenerate orbitals and 27 % in **3** for its nondegenerate HOMO. This raises the question as to how useful frontier orbital theory, which focuses on the HOMO and the lowest-occupied molecular orbital (LUMO), will be for predicting reactivity in models for graphene and defect-containing graphene. The most reactive interior carbons have higher  $\bar{I}_{S,\min}$  values than do the peripheral C=C bonds in **1** and **2**, and lower than the C=C bonds in **3**, **4** and **5**. How will frontier orbital theory handle these different types of models? We are currently addressing this issue in a systematic manner for a variety of molecular systems [Bulat FA, Herrera B, Murray JS, Politzer P, in preparation].

#### Identification of favored second hydrogenation sites

We have included Table 5 to provide some insight into the effect of first hydrogenation upon further hydrogenation and to the site-specific preferences for second hydrogenation. In the case of **1H**, it is difficult to identify sites on the side of the model with the hydrogen [20], which masks some of them, and so the  $\bar{I}_{S,\min}$  data in Table 5 for **1H** refer to the side of the coronene framework opposite to the hydrogen. However, in the nonplanar models **2–5** this is not a problem,

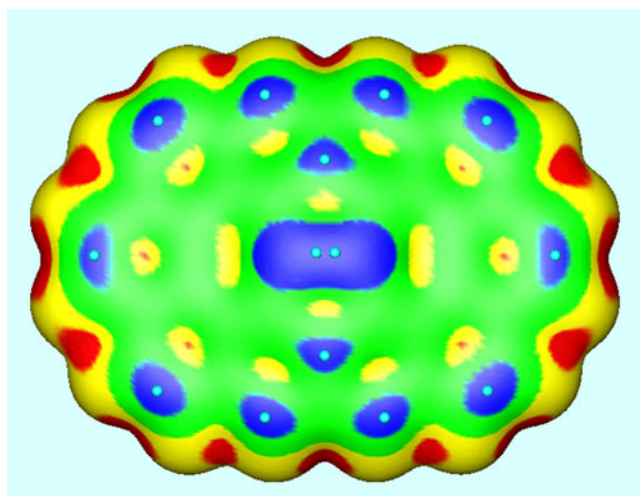


**Fig. 6** Computed  $\bar{I}_S(r)$  on the convex 0.001 au molecular surface of inverse Stone-Thrower-Wales defect-containing model **4**. Color ranges (eV): *blue*  $< 9.5$ ; *green* 9.5–11.0; *yellow* 11.0–12.0; *red*  $> 12.0$ . The locations of the  $\bar{I}_{S,\min}$  less than 9.5 eV are given by *light blue hemispheres*

presumably due to the curvature of the region around  $C_1$ , which allows one to visualize the adjacent carbon  $\bar{I}_{S,\min}$  on the 0.001 au contour of the electronic density. Since the convex-side carbon  $\bar{I}_{S,\min}$  of **2H**–**5H** are smaller in magnitude than are those for their concave sides, as has also been shown to be the case for **2** and **3** in Table 2 and Figs. 3 and 4, only the convex-side interior  $\bar{I}_{S,\min}$  are recorded in Table 5.

We find that in each system the lowest  $\bar{I}_{S,\min}$  correspond to carbons adjacent to  $C_1$ . And, except for the case of cap model **5H**, these  $\bar{I}_{S,\min}$  are lower in magnitude than the most reactive interior sites identified by  $\bar{I}_{S,\min}$  prior to hydrogenation. This suggests that further hydrogenation is favored for pristine and defect-containing graphene models such as **1H**–**4H**. For **1H** and **2H**, the lowest interior  $\bar{I}_{S,\min}$  correspond to the sites of the two carbons adjacent to  $C_1$ . This pattern has been observed for the second hydrogenation and

**Table 4** Computed  $\bar{I}_{S,\min}$  values, in eV, at positions corresponding to  $C_1$  of **1**–**5** on molecular surfaces corresponding to the 0.001 au, 0.003 au and 0.005 au contours of the electronic density. In parenthesis after each  $\bar{I}_{S,\min}$  value is the distance in Å from the carbon nucleus to the respective molecular surface. The van der Waals radius of carbon is 1.70 Å

Molecular system	$\bar{I}_{S,\min}$ (0.001 au)	$\bar{I}_{S,\min}$ (0.003 au)	$\bar{I}_{S,\min}$ (0.005 au)
<b>1</b>	9.89 (1.97)	10.23 (1.68)	10.42 (1.55)
<b>2</b>	9.24 (1.94)	9.57 (1.66)	9.73 (1.52)
<b>3</b>	8.08 (2.00)	8.44 (1.69)	8.63 (1.55)
<b>4</b>	8.14 (2.04)	8.52 (1.70)	8.71 (1.55)
<b>5</b>	7.49 (1.97)	7.78 (1.69)	7.92 (1.56)

**Table 5** Computed 0.001 au  $\bar{I}_{S,\min}$  values for the most reactive interior carbons of the monohydrogenated systems **1H**–**5H**, where the hydrogen is attached to one of the  $C_1$  carbons in parent systems **1**–**5**.  $C_a$  refers to an interior carbon adjacent to  $C_1$

Molecular system	Side	Position	$\bar{I}_{S,\min}$ (eV)
<b>1H</b>	Opposite to H	$C_{a,\text{interior}}$ (ortho)	9.17
<b>2H</b>	Same side as H	$C_{a,\text{interior}}$	9.04
<b>3H</b>	Same side as H	$C_a$ (other $C_1$ )	7.60
<b>4H</b>	Same side as H	$C_a$ (other $C_1$ )	8.02
<b>5H</b>	Same side as H	$C_a$	7.78

fluorination of coronene and a larger pristine graphene model [20] and in the second chlorination of a (5,5) carbon nanotube model [22], with the larger systems having the third adjacent carbon also activated. In **1** and **2**, these third adjacent carbons are along the perimeters, and thus have not been included in Table 5. In **3H** and in **4H**, the region of lowest  $\bar{I}_{S,\min}$  is the site of the adjacent  $C_1$  carbon. In these systems, this second  $C_1$  site is the one with the greatest degree of nonplanarity; the sums of these C– $C_1$ –C angles in **3H** and **4H** are  $\sim 340^\circ$  compared to  $\sim 359^\circ$  for the sums of the angles around the other two carbons adjacent to the carbon bearing the hydrogen), and from earlier arguments would be predicted to be the most reactive. Our results confirm this, as is seen in Table 5 and in Fig. 7 for **4H**. For hydrogenated cap model **5H**, the three carbons adjacent to  $C_1$  are those with the lowest  $\bar{I}_{S,\min}$ . The fact that the magnitudes of the  $\bar{I}_{S,\min}$  of these adjacent carbons in **5H** are higher than the  $C_1$  site in **5** may be due to these having less curvature than  $C_1$ .

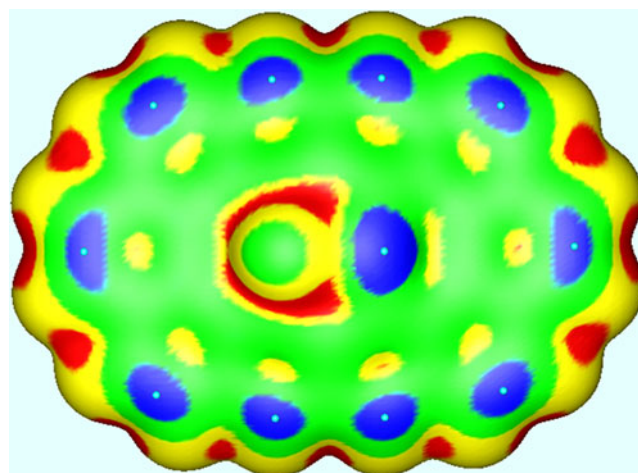


**Fig. 7** Computed  $\bar{I}_S(r)$  on the convex 0.001 au molecular surface of hydrogenated inverse Stone-Thrower-Wales defect-containing model **4H**, with the hydrogen attached to one of the central carbons fusing the two pentagons. Color ranges (eV): *blue*  $< 9.5$ ; *green* 9.5–11.0; *yellow* 11.0–12.0; *red*  $> 12.0$ . The locations of the  $\bar{I}_{S,\min}$  less than 9.5 eV are given by *light blue hemispheres*



## Summary

Our objectives in this study have been both general and specific: (1) to further explore the use of  $\bar{I}(\mathbf{r})$  in its third decade of use as a computational tool in identifying sites in molecular systems with reactive electrons, and (2) to specifically study how well  $\bar{I}(\mathbf{r})$  computed on molecular surfaces can predict the sites of reactive electrons in nonplanar defect-containing model graphene systems.  $\bar{I}(\mathbf{r})$  is computed easily on molecular surfaces defined by outer contours of the electronic density, such as the 0.001 au, and such surface representations, labeled  $\bar{I}_S(\mathbf{r})$ , allow one to look at all sites on the system with one calculation. This feature is particularly useful for large systems, such as nanotube and graphene models [20–22]. In our earlier studies [1, 4–9, 15, 16] and in more recent investigations of large carbon framework systems [20–22], we have identified the locations of the local surface minima, the  $\bar{I}_{S,\min}$ , as sites with the most reactive electrons, and thus those that are likely to be sites for substitution or addition reactions.

In this study, we extended our analysis of  $\bar{I}(\mathbf{r})$  to model systems corannulene (2), two inverse Stone-Thrower-Wales defect-containing models 3 and 4, and a nanotube cap model 5, all of which have one or more pentagons and which are nonplanar. Coronene (1) has been included as a reference non-defect-containing graphene model. To support our  $\bar{I}_S(\mathbf{r})$  predictions, we have computed the reaction energies for hydrogenation at all of the interior carbon sites that have local surface minima,  $\bar{I}_{S,\min}$ , in the smaller models 1–3, and at the most reactive interior carbons, identified as the positions of the  $\bar{I}_{S,\min}$  with lowest values, in 4 and 5. The reaction energies are more negative as the  $\bar{I}_{S,\min}$  at the site before hydrogenation is smaller in magnitude (more reactive electrons).

The predictions given by our computed  $\bar{I}_S(\mathbf{r})$  are obtained only by looking at the system before it reacts, and therefore do not account for any stabilization or destabilization in forming the hydrogenated product. In spite of this, we find good relationships between  $\Delta E$  and  $\bar{I}_{S,\min}$ , both within a particular framework such as 3 and in comparing the most reactive sites in 1–5. This may be because the differences in the nonplanarities of the sites before and after hydrogenation, as measured by the summation of C–C<sub>1</sub>–C angles before and after hydrogenation (Table 3), fall in a small range. The net result is that the  $\bar{I}_{S,\min}$  in models 1–5 are good indicators of the relative  $\Delta E$  for first hydrogenation. In regard to further hydrogenation, our computed  $\bar{I}_S(\mathbf{r})$  for 1H–5H suggest that interior carbons adjacent to the sites of first hydrogenation are the ones most activated toward further addition; in models 3 and 4, these are the sites of the other C<sub>1</sub> carbons with high local curvature.

A practical finding that has emerged from this study is that  $\bar{I}_S(\mathbf{r})$  computed on 0.001 au, 0.003 au and 0.005 au

contours of the electronic density yields results with similar trends with respect to the sites and the magnitudes of the lowest  $\bar{I}_{S,\min}$ . This provides support for utilizing contours of the electronic density yielding surfaces closer to the nuclei than the 0.001 au in cases where such surfaces may aid visualization, such as for sites for second or further addition.

**Acknowledgments** We are thankful for the continued support and guidance that we receive from Peter Politzer, to whom this paper is dedicated.

## References

- Sjoberg P, Murray JS, Brinck T, Politzer P (1990) *Can J Chem* 68:1440–1443
- Koopmans TA (1934) *Physica* 1:104–113
- Nesbet RK (1965) *Adv Chem Phys* 9:321–363
- Politzer P, Abu-Awwad F, Murray JS (1998) *Int J Quantum Chem* 69:607–613
- Murray JS, Seminario JM, Politzer P, Sjoberg P (1990) *Int J Quantum Chem Quantum Chem Symp* 24:645
- Brinck T, Murray JS, Politzer P, Carter RE (1991) *J Org Chem* 56:2934–2936
- Murray JS, Brinck T, Politzer P (1991) *Int J Quantum Chem Quantum Biol Symp* 40(S18):91–98
- Brinck T, Murray JS, Politzer P (1991) *J Org Chem* 56:5012–5015
- Murray JS, Brinck T, Politzer P (1992) *J Mol Struct (THEOCHEM)* 225:271–281
- Politzer P, Murray JS, Grice ME, Brinck T, Ranganathan S (1991) *J Chem Phys* 95:6699–6704
- Politzer P, Murray JS, Grice ME (2005) *Coll Czech Chem Comm* 70:550–558
- Politzer P, Shields ZP-I, Bulat FA, Murray JS (2011) *J Chem Theory Comput* 7:377–384
- Politzer P, Murray JS (2007) In: Toro-Labbé A (ed) *Chemical reactivity*, vol 8. Elsevier, Amsterdam, 119–137
- Politzer P, Murray JS, Bulat FA (2010) *J Mol Model* 16:1731–1742
- Brinck T, Murray JS, Politzer P (1993) *Int J Quantum Chem* 48:73–88
- Politzer P, Murray JS, Concha MC (2002) *Int J Quantum Chem* 88:19–27
- Politzer P, Murray JS (2012) *Theor Chem Accounts* 121:1114, 1–10
- Murray JS, Abu-Awwad F, Politzer P (2000) *J Mol Struct (THEOCHEM)* 501–502:241–250
- Peralta-Inga Z, Murray JS, Grice ME, Boyd S, O'Connor CJ, Politzer P (2001) *J Mol Struct (THEOCHEM)* 549:147–158
- Bulat FA, Burgess JS, Matis BR, Baldwin JW, Macaveiu L, Murray JS, Politzer P (2012) *J Phys Chem A* 116:8644–8652. doi:10.1021/jp3053604
- Dinadayalane TC, Murray JS, Concha MC, Politzer P, Leszczynski J (2010) *J Chem Theory Comput* 6:1351–1357
- Saha S, Dinadayalane TC, Leszczynska D, Murray JS, Leszczynski J (2012) *J Phys Chem C* 116:22399–22410. doi:10.1021/jp307090t
- Barth WE, Lawton RG (1966) *J Am Chem Soc* 88:380–381
- Hedberg L, Hedberg K, Cheng P-C, Scott LT (2000) *J Phys Chem A* 104:7689–7694
- Slayden SW, Liebman JF (2001) *Chem Rev* 101:1541–1566
- Scott LT, Bronstein HE, Preda DV, Ansems RBM, Bratchen MS,



- Hagen S (1999) *Pure Appl Chem* 71:209–219
27. Lusk MT, Carr DC (2008) *Phys Rev Lett* 100:175503, 1–4
  28. Lusk MT, Carr DC (2009) *Carbon* 47:2226–2232
  29. Lusk MT, Wu DT, Carr DC (2010) *Phys Rev B* 81:15544, 1–9
  30. Dinadayalane TC, Leszczynski J (2010) *Struct Chem* 21:1156–1169
  31. Politzer P, Lane P, Concha MC, Murray JS (2005) *Microelectron Eng* 81:485–493
  32. Robinson JT, Burgess JS, Junkermeier CE, Badescu SC, Reinecke TL, Perkins FK, Salalutdniov MK, Baldwin JW, Cuthbertson JC, Shhehan PE et al (2010) *Nano Lett* 10:3001–3005
  33. Teillet-Billy D, Rougeau N, Ivanovskaya VV, Sidis V (2010) *Int J Quantum Chem* 110:2231–2236
  34. Hernández Rosas JJ, Ramírez Gutiérrez RE, Escobedo-Morales A, Chigo Anotá E (2011) *J Mol Model* 17:1133–1139
  35. Wang Y, Qian H-J, Morokuma K, Irle S (2012) *J Phys Chem A* 116:7154–7160
  36. Frisch MJ, Trucks GW, Schlegel HB, Scuseria GE, Robb MA et al (2009) *Gaussian 09*, Revision A.1. Gaussian, Wallingford
  37. Bulat FA, Toro-Labbé A, Brinck T, Murray JS, Politzer P (2010) *J Mol Model* 16:1679–1691
  38. Bader RWF, Carrol MT, Cheeseman JR, Chang C (1987) *J Am Chem Soc* 109:7968–7979
  39. Baskin Y, Meyer L (1955) *Phys Rev* 100:544
  40. Allen FH, Kennard O, Watson DG, Brammer L, Guy Orpen A, Taylor R (1987) *J Chem Soc Perk Trans II*:S1-S19
  41. Dinadayalane TC, Leszczynski J (2007) *Chem Phys Lett* 434:86–91
  42. Boukhvalov DW, Katsnelson MI (2008) *Nano Lett* 8:4373–4379